Engineering Fracture Mechanics 77 (2010) 3625–3634

Contents lists available at ScienceDirect

Engineering Fracture Mechanics

journal homepage: www.elsevier.com/locate/engfracmech

A continuum phase field model for fracture

Charlotte Kuhn *, Ralf Müller

Technische Universität Kaiserslautern, P.O.B. 3049, D-67653 Kaiserslautern, Germany

ARTICLE INFO

Article history:
Available online 12 August 2010

Keywords:
Fracture
Phase field
Energy-momentum tensor (Eshelby tensor)
Energy release rate
$\mathcal{J}$-integral
Finite elements

ABSTRACT

A phase field model based on a regularized version of the variational formulation of brittle fracture is introduced. The influences of the regularization parameter that controls the interface width between broken and undamaged material and of the mobility constant of the evolution equation are studied in finite element simulations. A generalized Eshelby tensor is derived and analyzed for mode I loading in order to evaluate the energy release rate of the diffuse phase field cracks. The numerical implementation is performed with finite elements and an implicit time integration scheme. The configurational forces are computed in a postprocessing step after the coupled problem of mechanical balance equations and the evolution equation is solved. Some of the numerical results are compared to analytical results from classical Griffith theory.

1. Introduction

A variational free-discontinuity formulation of brittle fracture was given by Francfort and Marigo [1], where the total energy is minimized with respect to the crack geometry and the displacement field simultaneously. This formulation overcomes the limitations of the classical Griffith theory [2] as the entire evolution of cracks including their initiation and branching is determined by this minimization principle requiring no further criterion. However, a direct numerical discretization of the model faces considerable difficulties as the displacement field is discontinuous in the presence of cracks.

A regularized approximation of the model, which is more suitable for a numerical treatment, has been presented by Bourdin in [3,4]. The underlying theory of Γ-convergence is exposed e.g. in [5]. An additional field variable s is introduced to model changes in the stiffness of the material and to avoid the necessity of dealing with sharp interfaces. To minimize the regularized energy expression Bourdin suggests a so called alternate minimizations algorithm together with a backtracking procedure to satisfy a global optimality criterion with respect to the time evolution. Instead of this approach, we reinterpret the variable s as an order parameter of a phase field model with an evolution equation of the Ginzburg–Landau type, similar to earlier phase field models for fracture, e.g. [6,7]. The application of a phase field approach to crack propagation is possible with some modifications, taking the irreversible character of crack propagation into account.

2. A phase field model for fracture

2.1. The regularized fracture model

In the regularized model, cracks are represented by a field variable s which is *1* if the material is undamaged and *0* if there is a crack. Thus the variable s can be viewed as a damage parameter in elastic damage models. The total energy E of a linear elastic body with stiffness tensor $\mathbb{C}$ and crack resistance $\mathcal{G}_c$ depends on the displacement field $\boldsymbol{u}$ and the crack indicator s

* Corresponding author. Tel.: +49 631 205 2125; fax: +49 631 205 2128.
E-mail address: chakuhn@rhrk.uni-kl.de (C. Kuhn).

0013-7944/$ - see front matter © 2010 Elsevier Ltd. All rights reserved.
doi:10.1016/j.engfracmech.2010.08.009

$$E(\boldsymbol{u},s)=\int_\Omega \underbrace{\frac{1}{2}(s^2+\eta)\varepsilon(\boldsymbol{u}):[\mathbb{C}\varepsilon(\boldsymbol{u})]+\mathscr{G}_c\left(\frac{(1-s)^2}{4\epsilon}+\epsilon|\nabla s|^2\right)}_{=\Psi(\varepsilon,s)}dV. \tag{1}$$

In Eq. (1) the potential of external loads is neglected for the sake of simplicity only. The first term in Eq. (1) is the elastic strain energy density. The infinitesimal strain tensor ε is related to the displacement field $\boldsymbol{u}$ by

$$\varepsilon(\boldsymbol{u})=\frac{1}{2}\left(\nabla\boldsymbol{u}+(\nabla\boldsymbol{u})^T\right) \tag{2}$$

and the elastic stresses σ are derived from the energy density Ψ by

$$\sigma=\frac{\partial\Psi}{\partial\varepsilon}=(s^2+\eta)\mathbb{C}\varepsilon. \tag{3}$$

The factor $(s^2+\eta)$ models the stiffness loss between an undamaged ($s=1$) and a broken material ($s=0$). The term $\eta\mathbb{C}$ with $0<\eta\ll 1$ is the residual stiffness if $s=0$. For numerical reasons (stability) η may not be chosen too small. However, too large values for η overestimate the bulk energy in fractured zones. In the absence of volume forces, the equilibrium condition reads

$$\mathrm{div}\sigma=\boldsymbol{0}. \tag{4}$$

The second term in Eq. (1) represents the surface/crack energy. The width of the transition area between undamaged solid and broken material is controlled by the parameter ϵ which has the dimension of a length [8]. With ϵ tending to zero, the transition area turns into a sharp interface and the regularized energy converges to the original energy expression by Francfort and Marigo which is the same as in classical Griffith fracture mechanics.

2.2. Phase field formulation

Interpreting s as an order parameter of a phase field model, we supplement Bourdin's formulation by a Ginzburg–Landau type evolution equation which is derived from the energy density Ψ [9] and governs the evolution of s with respect to time:

$$\dot{s}=-M\frac{\delta\Psi}{\delta s}=-M\left(s\varepsilon:[\mathbb{C}\varepsilon]-2\mathscr{G}_c\epsilon\Delta s+\frac{1}{2}\frac{\mathscr{G}_c}{\epsilon}(s-1)\right), \tag{5}$$

where $M\geqslant 0$ is a mobility constant. Eq. (5) has to be slightly modified in order to take account of the irreversible character of crack propagation. Two different strategies to avoid crack healing are possible:

- either fix s, if it is close to *0*,
- or set $\dot{s}$ to *0*, if $\frac{\delta\Psi}{\delta s}<0$, so that $\dot{s}\leqslant 0$ holds.

The first alternative is used in the simulations of Section 4.

2.3. 1D stationary problem

To get a better understanding of the meaning of ϵ, the 1D example of a bar of length $2L$ with a crack in the centre is analyzed. Neglecting the elastic energy and considering a stationary problem Eq. (5) yields in

$$-\frac{1}{2}=-\frac{s(x)}{2}+2\epsilon^2 s''(x) \tag{6}$$

with $-L\leqslant x\leqslant +L$. The solution with a crack in the centre (at $x=0$) is given by

$$s^{\pm}(x)=1-\cosh\left(\frac{x}{2\epsilon}\right)\pm\coth\left(\frac{L}{2\epsilon}\right)\sinh\left(\frac{x}{2\epsilon}\right), \tag{7}$$

where + applies for $x\geqslant 0$ and − for $x<0$, respectively. Fig. 1 shows a plot of the solution $s(x)$ for different values of ϵ. Large values of ϵ smoothen the crack field, whereas the limit $\epsilon\to 0$ yields a discontinuous function which is *0* at $x=0$ and *1* elsewhere. Inserting the solution $s(x)$ into the expression for the surface energy, one can recover the crack resistance $\mathscr{G}_c$ letting $\epsilon\to 0$.

$$E^{\mathrm{surf}}=\mathscr{G}_c\int_{-L}^{+L}\frac{(1-s)^2}{4\epsilon}+\epsilon s'^2dx \tag{8}$$

$$=\frac{\mathscr{G}_c}{2}\left(\coth\left(\frac{L}{2\epsilon}\right)+\coth\left(\frac{L}{2\epsilon}\right)\right)\overset{\epsilon\to 0}{=}\mathscr{G}_c \tag{9}$$

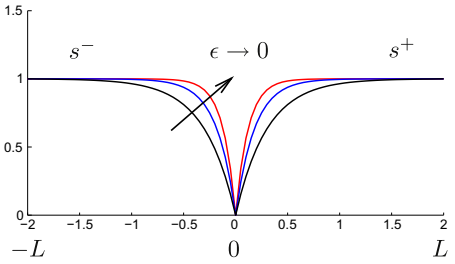

Fig. 1. Cracked bar.

2.4. Generalization of the Eshelby tensor

Francfort and Marigo's formulation of brittle fracture is conceptually close in spirit to the classical Griffith model where crack growth arises from a competition of elastic energy released and an increase of surface energy. In order to account for this variational character of the underlying material model, a method to calculate the energy release rate of the diffuse phase field cracks is proposed following the derivations in [10]. The concept of configurational forces provides a convenient method to compute the energy release rate of an elastic body numerically within the FE method. With some extensions this approach is also applicable for phase field models.

As the classical Eshelby tensor for linear elastic bodies the generalized Eshelby tensor can be obtained by chain rule differentiation of the energy density Ψ. Additional terms emerge from the dependance of the energy on the crack field s and its gradient.

$$\nabla\Psi = \frac{\partial\Psi}{\partial\varepsilon}\nabla\varepsilon + \frac{\partial\Psi}{\partial s}\nabla s + \frac{\partial\Psi}{\partial\nabla s}\nabla\nabla s + \frac{\partial\Psi}{\partial \boldsymbol{x}}|_{\text{expl.}} \tag{10}$$

Using static equilibrium (4), the strain displacement relation (2), and the evolution Eqs. (5), (10) yields the configurational force balance

$$\operatorname{div}\widetilde{\boldsymbol{\Sigma}} + \boldsymbol{g} = 0, \tag{11}$$

where the generalized Eshelby tensor $\widetilde{\boldsymbol{\Sigma}}$ and the configurational body force $\boldsymbol{g}$ are given by

$$\widetilde{\boldsymbol{\Sigma}} = \Psi\mathbf{1} - \nabla\boldsymbol{u}^T\sigma - \frac{\partial\Psi}{\partial\nabla s}\nabla s \qquad \text{and} \tag{12}$$

$$\boldsymbol{g} = \frac{\dot{s}}{M}\nabla s - \frac{\partial\Psi}{\partial \boldsymbol{x}}|_{\text{expl.}}. \tag{13}$$

In order to see the connection to the classical Eshelby tensor the generalized Eshelby tensor is decomposed into two parts that are assigned to the elastic part Ψ^{el} and the surface part Ψ^{surf} of the energy density.

$$\begin{aligned}
&\widetilde{\boldsymbol{\Sigma}}^{\text{el}} = \Psi^{\text{el}}\mathbf{1} - \nabla\boldsymbol{u}^T\sigma \quad \text{with} \quad \Psi^{\text{el}} = \frac{1}{2}(s^2+\eta)\varepsilon : \mathbb{C}\varepsilon \qquad \text{and}\\
&\widetilde{\boldsymbol{\Sigma}}^{\text{surf}} = \Psi^{\text{surf}}\mathbf{1} - \frac{\partial\Psi}{\partial\nabla s}\nabla s \quad \text{with} \quad \Psi^{\text{surf}} = \mathscr{G}_c\left(\epsilon|\nabla s|^2 + \frac{(1-s)^2}{4\epsilon}\right).
\end{aligned} \tag{14}$$

In intact material, where the crack field $s \equiv 1$, the surface part of the energy density as well as the surface part $\widetilde{\boldsymbol{\Sigma}}^{\text{surf}}$ of the generalized Eshelby tensor vanish and the elastic parts coincide with the classical Eshelby tensor and the usual elastic energy of Hookean material, respectively.

The configurational force acting on the crack tip can be computed as the integral of the configurational body force $\boldsymbol{g}$ over a sufficiently large domain Ω_0 around the crack tip as depicted in Fig. 2. As $\boldsymbol{g}$ and $\widetilde{\boldsymbol{\Sigma}}$ are well defined everywhere, there is no need to exclude the crack from the domain of integration. The divergence theorem permits to rewrite the integral of the divergence of $\widetilde{\boldsymbol{\Sigma}}$ as a contour integral over the boundary $\partial\Omega_0$ of the domain Ω_0 with $\boldsymbol{n}$ being the outer normal vector.

$$\int_{\Omega_0}\boldsymbol{g}dV = -\int_{\Omega_0}\operatorname{div}\widetilde{\boldsymbol{\Sigma}}dV = -\int_{\partial\Omega_0}\widetilde{\boldsymbol{\Sigma}}\boldsymbol{n}ds = -\int_{\partial\Omega_0}\widetilde{\boldsymbol{\Sigma}}^{\text{el}}\boldsymbol{n}ds - \int_{\partial\Omega_0}\widetilde{\boldsymbol{\Sigma}}^{\text{surf}}\boldsymbol{n}ds \tag{15}$$

For a further investigation the contour $\partial\Omega_0$ is split in two sections $\partial\Omega_0|_{A\to B}$ and $\partial\,\Omega_0|_{B\to A}$ according to Fig. 2. In a mode I loading situation the elastic energy Ψ^{el} and the stresses σ and therefore $\widetilde{\boldsymbol{\Sigma}}^{\text{el}}$ vanish on $\partial\Omega_0{-}_{B\to A}$ and thus

$$\int_{\partial\Omega_0}\widetilde{\boldsymbol{\Sigma}}^{\text{el}}\boldsymbol{n} = \int_{\partial\Omega_0|_{A\to B}}\widetilde{\boldsymbol{\Sigma}}^{\text{ el}}\boldsymbol{n}. \tag{16}$$

As $\widetilde{\boldsymbol{\Sigma}}^{\text{el}}$ coincides with the classical Eshelby tensor where $s \equiv 1$, the first component of Eq. (16) is found to be Rice's $\mathscr{J}$-integral [11] that is equal to the energy release rate of a mode I crack.

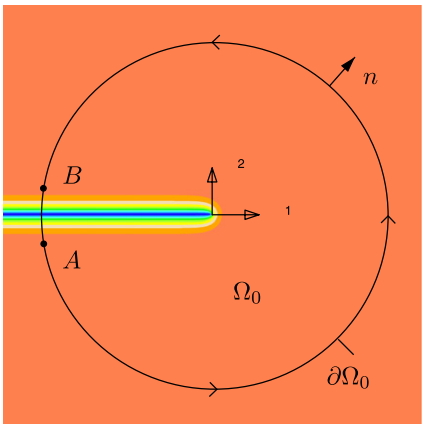

Fig. 2. Contour of s with integration domain.

The additional surface component vanishes on $\partial\Omega_0|_{A\to B}$ and the integral over $\partial\,\Omega_0|_{B\to A}$ can be evaluated using the results from the one dimensional problem discussed in the previous Section 2.3.

$$\int_{\partial\Omega_0}\widetilde{\boldsymbol{\Sigma}}^{\text{surf}}\boldsymbol{n}ds=\int_{\partial\Omega_0|_{B\to A}}\widetilde{\boldsymbol{\Sigma}}^{\text{surf}}\boldsymbol{n}ds=-\int_{\partial\Omega_0|_{B\to A}}\begin{pmatrix}\Psi^{\text{surf}}\\0\end{pmatrix}ds=-\begin{pmatrix}\mathscr{G}_c\\0\end{pmatrix}\tag{17}$$

For a more detailed discussion (also including mode II loading) the reader is referred to [10].

3. Numerical implementation

3.1. Finite element formulation

The fracture model is implemented into a finite element framework with the displacements $\boldsymbol{u}$ and the order parameter s as nodal degrees of freedom. With virtual displacements $\delta\boldsymbol{u}$ and δs, the weak forms of Eqs. (4) and (5) read

$$\int_\Omega\nabla\delta\boldsymbol{u}\cdot\sigma dV=\int_{\partial\Omega_t}\delta\boldsymbol{u}\cdot\boldsymbol{t}_n^*dA\tag{18}$$

and

$$\int_\Omega\left[\delta s\frac{\dot{s}}{M}-\nabla\delta s\cdot\boldsymbol{q}+\delta s\left(s\varepsilon:[\mathbb{C}\varepsilon]+\frac{\mathscr{G}_c}{2\epsilon}(s-1)\right)\right]dV=\int_{\partial\Omega_q}\delta sq_n^*dA\tag{19}$$

with $\boldsymbol{q}=-2\mathscr{G}_c\epsilon\nabla s$. The boundary conditions for the stresses σ and for $\boldsymbol{q}$ are prescribed by the traction $\boldsymbol{t}_n^*$ and the normal flux q_n^*.

In a 2D setting using Voigt-notation – denoted by an underbar in the following – the discretization of $\boldsymbol{u}$ and s with shape functions N_I for node I is given by

$$\underline{\boldsymbol{u}}=\sum_{I=1}^{N}N_I\hat{\underline{\boldsymbol{u}}}_I,\qquad\underline{\varepsilon}=\sum_{I=1}^{N}[\underline{B}_I^{\boldsymbol{u}}]\hat{\underline{\boldsymbol{u}}}_I,\tag{20}$$

$$s=\sum_{I=1}^{N}N_I\hat{s}_I,\qquad\underline{\nabla s}=\sum_{I=1}^{N}[\underline{B}_I^{s}]\hat{s}_I,\tag{21}$$

with

$$[\underline{B}_I^{\boldsymbol{u}}]=\begin{bmatrix}N_{I,x}&0\\0&N_{I,y}\\N_{I,y}&N_{I,x}\end{bmatrix}\qquad\text{and}\qquad[\underline{B}_I^{s}]=\begin{bmatrix}N_{I,x}\\N_{I,y}\end{bmatrix}\tag{22}$$

Inserting these discretizations into the left hand sides of Eqs. (18) and (19), one obtains the residuals

$$[\underline{R}_I]=\begin{bmatrix}\underline{R}_I^{\boldsymbol{u}}\\R_I^{s}\end{bmatrix}=\int_\Omega\begin{bmatrix}[\underline{B}_I^{\boldsymbol{u}}]^T\underline{\sigma}\\N_I\frac{\dot{s}}{M}-[\underline{B}_I^{s}]^T\underline{\boldsymbol{q}}+N_I\left(s\underline{\varepsilon}^T\cdot(\underline{\mathbb{C}\varepsilon})+\frac{\mathscr{G}_c}{2\epsilon}(s-1)\right)\end{bmatrix}dV.\tag{23}$$

The stiffness matrix $[K_{IJ}]$ as well as the damping matrix $[D_{IJ}]$ are symmetric and given by

$$[\underline{K}_{IJ}] = \int_\Omega \begin{bmatrix} [\underline{B}^{\boldsymbol{u}}_I]^T(s^2+\eta)\underline{\mathbb{C}}[\underline{B}^{\boldsymbol{u}}_J] & [\underline{B}^{\boldsymbol{u}}_I]^T 2s\underline{\mathbb{C}}\underline{\varepsilon}N_J \\ N_I 2s(\underline{\mathbb{C}}\underline{\varepsilon})^T[\underline{B}^{\boldsymbol{u}}_J] & 2\mathscr{G}_c\epsilon[\underline{B}^s_I]^T[\underline{B}^s_J] + N_I\left(\underline{\varepsilon}^T\cdot\underline{\mathbb{C}}\underline{\varepsilon} + \frac{\mathscr{G}_c}{2\epsilon}\right)N_J \end{bmatrix} dV \tag{24}$$

and

$$\underline{D}_{IJ} = \int_\Omega \begin{bmatrix} 0 & 0 \\ 0 & \frac{1}{M}N_I N_J \end{bmatrix} dV. \tag{25}$$

Gauß quadrature is used to evaluate the integrals and the time integration of the transient terms is done with the backward Euler method. An automatic step size control is helpful for the simulations because of the rapidly decreasing stiffness during fracture.

3.2. Calculation of configurational forces

Starting point for the computation of discrete configurational forces is a weak formulation of the configurational force balance (11) as derived in [12,13]. With vectorial test functions $\boldsymbol{\eta}$ vanishing on the boundary $\partial\Omega$ of the considered body, this weak formulation reads

$$\int_\Omega \left[-\widetilde{\boldsymbol{\Sigma}} : \nabla\boldsymbol{\eta} + \boldsymbol{g}\cdot\boldsymbol{\eta}\right] dV = 0. \tag{26}$$

As usual in the FE method the test functions are discretized using their nodal values $\hat{\boldsymbol{\eta}}_I$ and shape functions N_I: $\boldsymbol{\eta} = \sum_{I=1}^N N_I\hat{\boldsymbol{\eta}}_I$. In order to account for the possible unsymmetry of the generalized Eshelby tensor, matrix notation is used for $\widetilde{\boldsymbol{\Sigma}}$ and the discretized form of Eq. (26) reads

$$\sum_{I=1}^N \left[\int_\Omega \left(\widetilde{\boldsymbol{\Sigma}}\nabla N_I - \boldsymbol{g}N_I\right) dV\right]\cdot\hat{\boldsymbol{\eta}}_I = 0. \tag{27}$$

As this equality must hold for any value of $\boldsymbol{\eta}$, the bracketed term must vanish defining $\int_\Omega \boldsymbol{g}N_I dV = \int_\Omega \widetilde{\boldsymbol{\Sigma}}\nabla N_I dV$ to be the discrete configurational force acting on node I.

4. Results

The model has been implemented into a quadrilateral plane strain element. In this section an illustrative mode I loading experiment is simulated and the results are examined from different points of view. In all calculations an isotropic material with Lamé constants $\lambda = \mu = 22\,\frac{\text{kN}}{\text{mm}^2}$ is considered. The decrease in stiffness is limited by $\eta = 10^{-5}$.

4.1. Mode I loading of a plate with initial crack

Fig. 3 shows the setup for a plate ($b = 10$ cm) with an initial crack under mode I loading which is used in the numerical simulations of this section. Exploiting the symmetry of the sample only the upper half of the structure is considered in the numerical model. Near the crack a uniform quadratic grid of mesh size $h = 0.3125$ mm is used for the discretization. The system is initially unstrained and then loaded by a linearly increasing tension

$$\sigma(t) = \sigma_0\cdot\frac{t}{t_0} \quad \text{with} \quad \frac{\sigma_0}{t_0} = 600\,\frac{\text{N}}{\text{cm}^2\,\text{s}}. \tag{28}$$

The initial crack is modeled by setting $s(x,y)$ to zero, where $0 \leqslant x \leqslant a$ and $y = 0$. However, this manipulation of the s-field produces an unstable situation, which is an undesirable starting point for the simulations. Therefore one static iteration is performed to find a stress free, stationary state ($\dot{s} = 0$) to start from. The contour plots in Fig. 4 show the situation before and after the static iteration step for $\epsilon = 6$ mm. The initially sharp line which indicates the crack in Fig. 4a) is smoothened in the stationary state shown in Fig. 4b. The parameter ϵ controls how much the initially sharp interface is smoothened in the static iteration step. This is also illustrated in Fig. 5. The plot shows nodal values of s along the positive y-axis in the stationary state for different values of ϵ. If ϵ is sufficiently small, the values are in good agreement with the analytic results obtained from the 1D stationary example of Section 2.3.

For the setup shown in Fig. 3 an analytical solution in terms of stress intensity factors is available in [14]:

$$K_I = \sigma\sqrt{\pi a}\sqrt{\frac{2b}{\pi a}\tan\left(\frac{\pi a}{2b}\right)}\cdot C\left(\frac{a}{b}\right) \tag{29}$$

with

$$C\left(\frac{a}{b}\right) = \frac{0.752 + 2.02\,\frac{a}{b} + 0.37\left(1-\sin\left(\frac{\pi a}{2b}\right)\right)^3}{\cos\left(\frac{\pi a}{2b}\right)}. \tag{30}$$

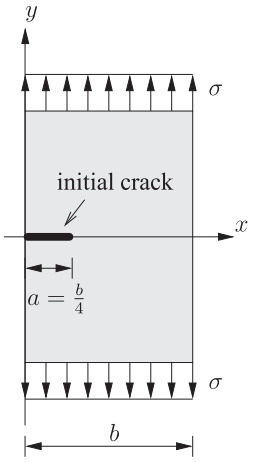

Fig. 3. Experimental setup.

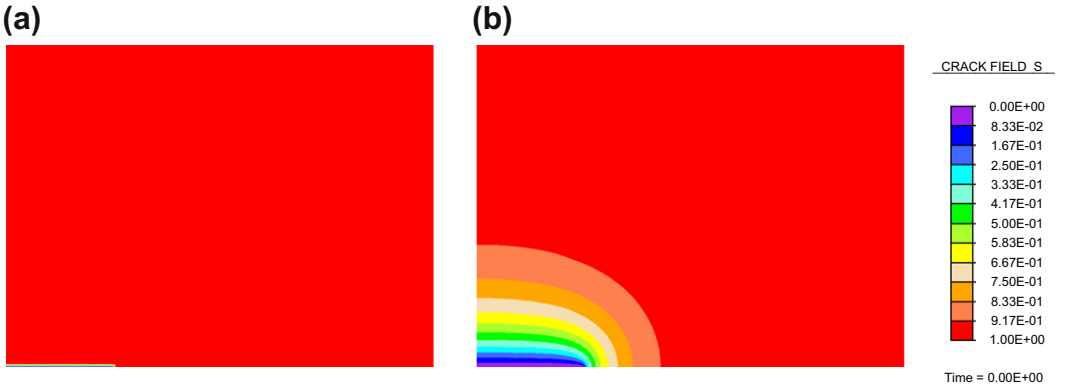

Fig. 4. Contour plots of s (a) before and (b) after the static iteration.

According to Griffith's criterion a crack will grow if the released strain energy is large enough to form the new crack surfaces. In a plane strain setting Griffith's crack growth criterion [2] reads

$$\frac{1-\nu^2}{E}K_I^2 \geqslant \mathcal{G}_c. \tag{31}$$

From Eq. (31) together with Eq. (29) the critical value σ_{crit} for the mode I stress load is given by

$$\sigma_{\text{crit}} = \sqrt{\frac{E}{1-\nu^2}\frac{\mathcal{G}_c}{2b\tan\left(\frac{\pi a}{2b}\right)}}\cdot C\left(\frac{a}{b}\right)^{-1}. \tag{32}$$

In the numerical simulation the stress load increases linearly with time and the crack growth should start at time $t_{\text{crit}} = \frac{\sigma_{\text{crit}}}{\sigma_0}t_0$. Fig. 6 shows how the numerical simulations compare with the analytical results for Griffith's model. Here the lengthscale parameter ϵ and the mobility constant M are

$$\epsilon = 0.625\text{mm} \qquad \text{and} \qquad M = 5.0\frac{\text{cm}^2}{\text{N}\cdot\text{s}}. \tag{33}$$

The crack resistance $\mathcal{G}_c$ is varied from 0.25 to $10.0\frac{\text{N}}{\text{mm}}$. The start of crack propagation is defined as the time when the s-value of the first node in front of the initial crack becomes zero. With the chosen values for the parameters ϵ and M the numerical values for the start of crack propagation lie close to the analytic curve from the Griffith criterion.

4.2. Influence of the mobility parameter M

The same example as in Section 4.1 was chosen to study the influence of the mobility constant M on the crack propagation behaviour. The parameter ϵ and the crack resistance $\mathcal{G}_c$ are held constant at

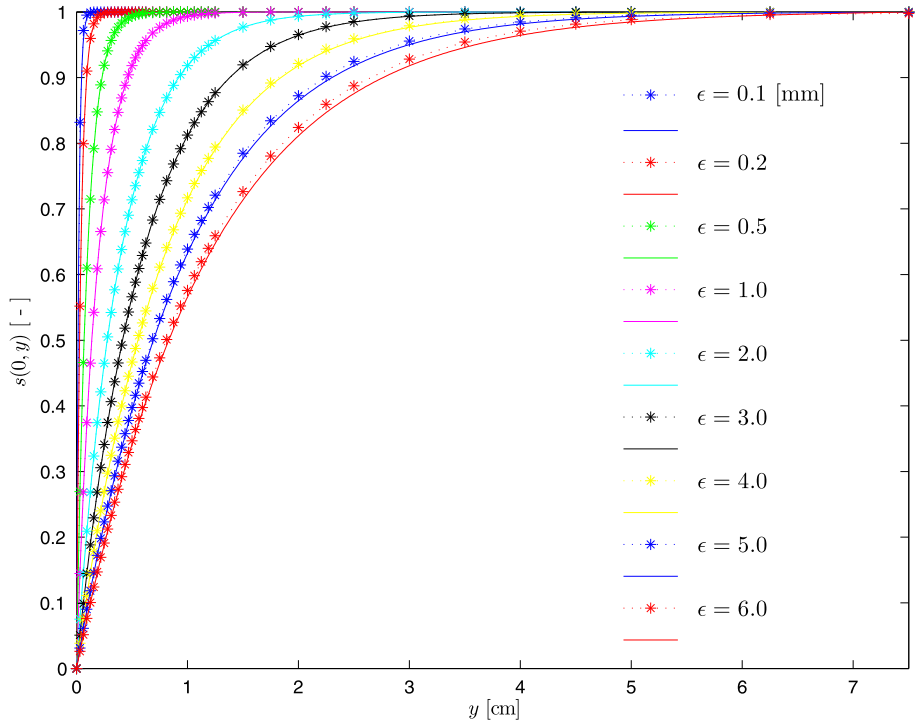

Fig. 5. Nodal values of s (stars) along the y-axis for different values of ϵ compared to the analytic 1D solution (solid line).

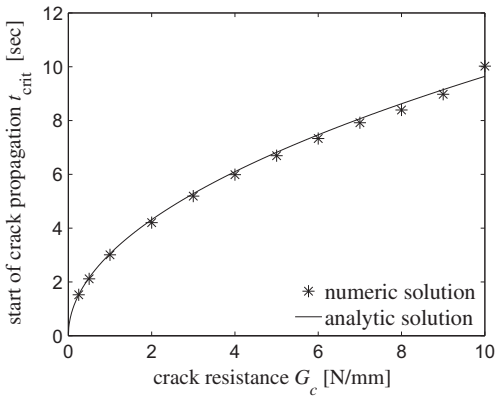

Fig. 6. Start of crack propagation for different values of $\mathscr{G}_c$ (stars) compared to the analytic solution (solid line).

$$\epsilon = 0.625 \text{ mm} \qquad \text{and} \qquad \mathscr{G}_c = 1.0 \frac{\text{N}}{\text{mm}}, \tag{34}$$

whereas the mobility M is varied in a range from *0.01* to $10 \frac{\text{cm}^2}{\text{N·sec}}$.

To track the crack tip the nodal values of the crack field s along the positive x-axis are recorded. The node with the largest x-coordinate where s equals zero is defined as the crack tip position.

The two plots of Fig. 7 show curves describing the crack tip position as a function of time for different values of M. The same stress loading as in the previous calculations was used in the simulations for Fig. 7a, whereas in the simulations for Fig. 7b a linearly increasing displacement loading was applied. Similarly for both loading cases, small values of M significantly delay the start of the crack propagation.

In the stress loading case (Fig. 7a) the crack grows instantaneously at time $t \approx 3$ s for any sufficiently large M. In this case the solution can be considered as stationary. In the transient solutions for smaller values of M, the crack tip velocity immediately after the start of the crack propagation is significantly dependent on M. However, after this starting phase, when the crack tip reaches the middle of the sample $x \approx 5$ cm the further cracking is almost instantaneous.

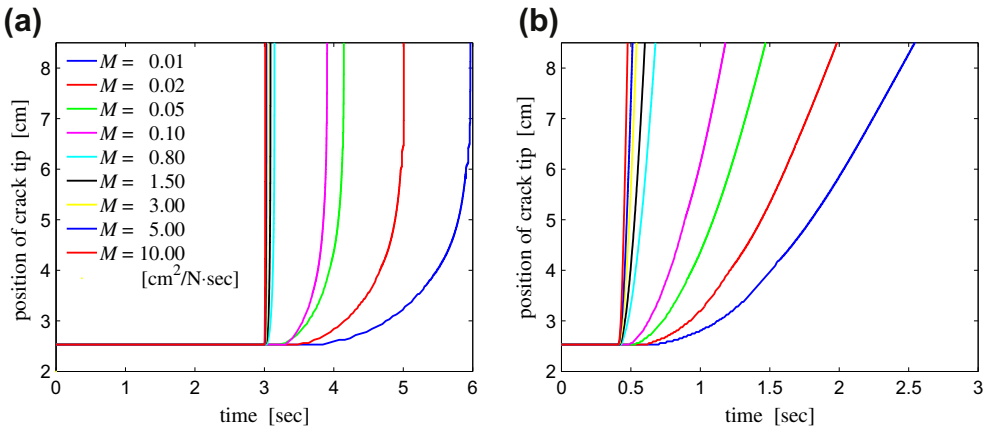

Fig. 7. Position of the crack tip versus time for (a) stress load and (b) displacement load.

In the displacement load simulations (Fig. 7b), stable crack growth can be observed and the crack tip velocity can be measured by finding the slope of the curve. After the crack tip passes $x = 5$ cm the velocity can be regarded as constant. A linear regression analysis of the curves where the crack tip position is between *5.0* and *8.5* cm gives the velocities shown in Fig. 8.

4.3. Configurational forces

In this last section the energy release rate during undercritical mode I loading is studied. The material parameters and the experimental setup are the same as in the previous example with phase field parameters

$$\epsilon = 2,0\,\text{mm} \qquad \text{and} \qquad M = 5\frac{\text{cm}^2}{\text{N}\cdot\text{s}}. \tag{35}$$

The arrows in Fig. 9 represent the discrete configurational forces $\int_\Omega \boldsymbol{g} N_I dV = \int_\Omega \widetilde{\boldsymbol{\Sigma}} \nabla N_I dV$ acting on the nodes surrounding the crack. Fig. 9a shows the initial state after the relaxation step. At this stage the configurational force acting on the crack tip can be interpreted as cohesive force that has to be overcome for the crack to propagate. Fig. 9b illustrates the situation just before the onset of crack propagation, when the cohesive part of the configurational force acting on the crack tip in x-direction is completely counterbalanced by the elastic part.

The evolution of the configurational forces acting on the crack tip in x-direction with respect to the loading is shown in Fig. 10. The diffuse crack interface requires to add up the discrete configurational forces in a sufficiently large area around the crack tip in order to get meaningful results. The forces acting in negative x-direction are plotted on the positive axis, because the negative x-component of the elastic part equals the $\mathcal{J}$-integral or the energy release rate, respectively. As to be expected from the derivations of Section 2.4 the cohesive part $\int_{\partial\Omega_0} \widetilde{\boldsymbol{\Sigma}}^{\text{surf}} \boldsymbol{n} ds$ remains constant at the critical value $-\mathcal{G}_c$, while the elastic part increases quadratically with the loading.

In this simulation the diffuse crack starts to propagate at a proportional load value of 0.74, just when the energy release rate reaches the critical value $\mathcal{G}_c$. Thus, the phase field model conserves this feature of the underlying variational formulation.

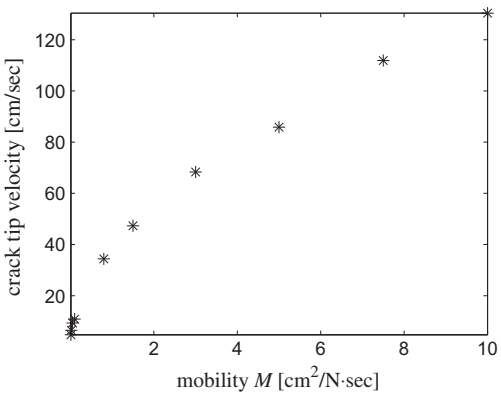

Fig. 8. Crack tip velocity versus mobility M.

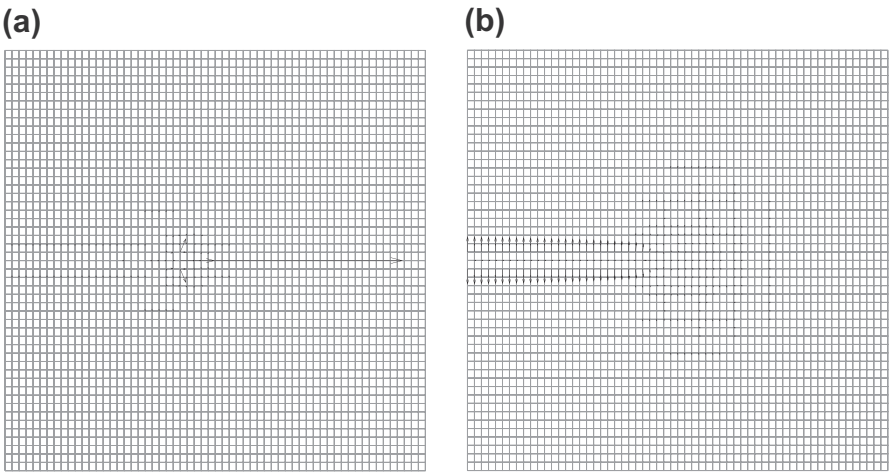

Fig. 9. Generalized configurational forces around the crack tip: (a) before loading and (b) just before the onset of crack propagation.

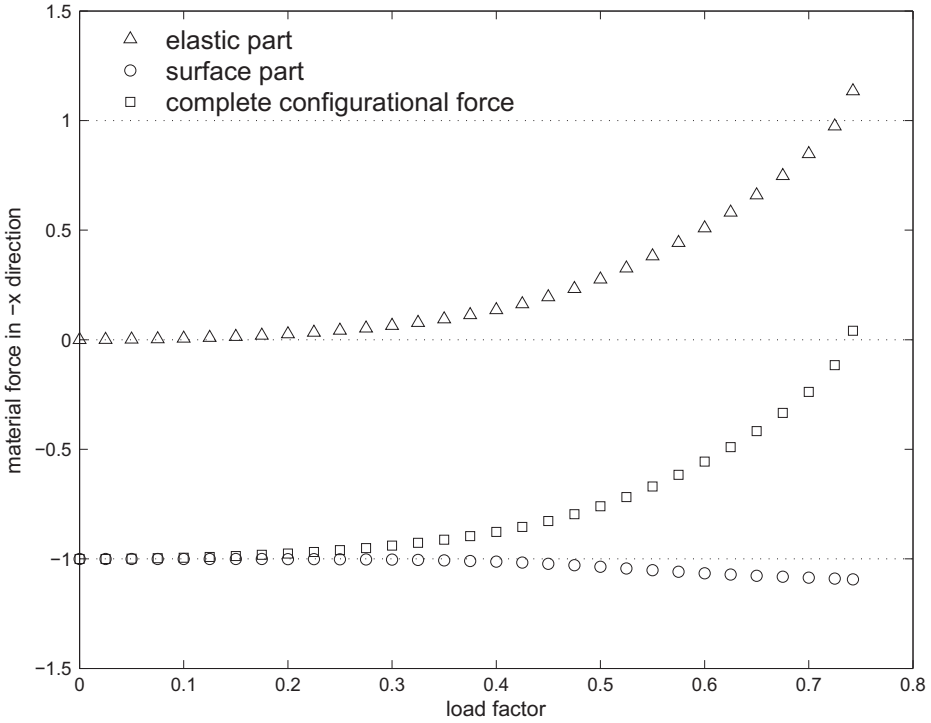

Fig. 10. Different parts of the configurational force acting on the crack tip plotted over the load factor.

5. Summary

Minimization of the total energy with respect to the displacement field and the crack field is the basic principle of Bourdin's regularized fracture model. Contrary to [3,4,15] where the minimization is performed with an alternate minimizations algorithm, we interpret the crack variable as the order parameter of a phase field model and address cracking as a phase transition problem. Therefore a Ginzburg–Landau type evolution equation and an additional parameter, the mobility M, had to be introduced to the model. The influence of this newly introduced constant on the crack propagation behaviour has been explored in a simple mode I simulation. Sufficiently large values produce quasi-stationary solutions which are in good agreement with the classical Griffith model, while small values of M significantly delay the crack propagation. A generalized version of the Eshelby tensor suited for phase field models has been derived in order to compute the energy release

rate of a mode I crack. Simulations have shown that the onset of crack propagation in the phase field model can be linked to the energy release rate reaching the critical value $\mathscr{G}_c$ just as in the variational formalism.

References

[1] Francfort GA, Marigo JJ. Revisiting brittle fracture as an energy minimization problem. J Mech Phys Solids 1998;46(8):1319–42.
[2] Griffith A. The phenomena of rupture and flow in solids. Phil Trans Roy Soc Lond 1921;221:163–98.
[3] Bourdin B. Numerical implementation of the variational formulation of quasi-static brittle fracture. Interfaces Free Bound 2007;9:411–30.
[4] Bourdin B, Francfort GA, Marigo JJ. The variational approach to fracture. J Elasticity 2008;91:5–148.
[5] Braides A. Γ-convergence for beginners. Oxford: Oxford University Press; 2002.
[6] Eastgate LO, Sethna JP, Rauscher M, Cretegny T. Fracture in mode I using a conserved phase-field model. Phys Rev 2002;E71:036117.
[7] Spatschek R, Hartmann M, Brener EA, Müller-Krumbhaar H. Phase field modeling of fast crack propagation. Phys Rev Lett 2006;96:015502.
[8] Spatschek R, Pilipenko D, Müller-Gugenberger C, Brener EA. Phase field modeling of fracture and composite materials. In: Proceedings of CDCM, Stuttgart, Germany; 2008.
[9] Ginzburg V, Landau L. On the theory of superconductivity. Zh Eksp Teor Fiz 1959;20:1064–82.
[10] Hakim V, Karma A. Laws of crack motion and phase-field models of fracture. J Mech Phys Solids 2009;57:342–68.
[11] Rice J. A path independent integral and approximate analysis of strain concentration by notches and cracks. J Appl Mech 1968;35(2):379–86.
[12] Müller R, Kolling S, Gross D. On configurational forces in the context of the finite element method. Int J Numer Methods Engng 2002;53(7):1557–75.
[13] Gross D, Kolling S, Müller R, Schmidt I. Configurational forces and their application in solid mechanics. Eur J Mech A/Solids 2003;22:669–92.
[14] Gross D, Seelig T. Fracture mechanics. Berlin, Heidelberg, New York: Springer; 2006.
[15] Del Piero G, Lancioni G, March R. A variational model for fracture: numerical experiments. J Mech Phys Solids 2007;55:2513–37.